



Section 8. Irradiation-induced restructuring (rim effect etc.)

Formation of the rim structure in high burnup fuelHj. Matzke^{*}, J. Spino*European Commission, Joint Research Centre, Institute for Transuranium Elements, Postfach 2340, D-76125 Karlsruhe, Germany***Abstract**

The process of grain subdivision or polygonization in UO_2 was studied by using ion irradiation techniques and by investigating the rim structure in high burnup UO_2 fuel. Ion irradiation with fission product ions caused first the formation of subgrain boundaries, observed in high resolution transmission electron microscopy, HRTEM. At higher doses, polygonization was completed at a well defined threshold. High burnup UO_2 fuel showing well developed rim zones was investigated in optical, scanning and transmission electron microscopy. The oxygen potential $\Delta\bar{G}(\text{O}_2)$, the hardness H and the fracture toughness K_{Ic} of the restructured material and the radial dependence of porosity, grain subdivision, H and K_{Ic} were measured. K_{Ic} was found to change at smaller radial positions than the other properties, indicating a nucleation process not affecting all properties to the same extent. The emerging picture for the formation of the rim structure in UO_2 is discussed. © 1997 Elsevier Science B.V.

1. Introduction

The peripheral region (the ‘rim’) of high burnup UO_2 fuel develops a particular microstructure known as the rim-structure [1–4]. These microstructural changes occur first when the cross-section averaged burnup exceeds about 40 GWd/tM. At fuel cross-section averaged burnups below ~ 60 GWd/tM, this structure is confined to a width of 150 to 200 μm , i.e., to the ‘rim region’ of the UO_2 pellets. In this region, the local burnup is increased exponentially towards the cladding where it is higher than the average value by a factor of up to ~ 2.5 . The reason is the local formation of fissile Pu-239 by resonance neutron capture of U-238. The obvious changes in the rim zone are grain subdivision (or polygonization), i.e., each as-sintered grain of typically ~ 5 – 10 μm size is subdivided into $\geq 10^4$ new small grains of ~ 0.15 to 0.3 μm size, and the formation of μm -sized pores. The new grains are depleted in fission gas which is mainly contained in the new pores.

While the above neutronic rim effect is restricted to a depth of 150–200 μm , the new structure has been found to extend deeper into the UO_2 pellets (e.g., Refs. [4–7]); e.g.,

in a fuel with cross-section averaged burnup of 74 GWd/tM it was found to a depth of 1650 μm [6]. In the present work results of ion irradiation experiments of UO_2 with fission products are presented. Ion irradiation has been used extensively to simulate the conditions of fission and to obtain basic data to better understand the parameters important for polygonization. Heavy ion tracks were observed in TEM and could be evaluated in terms of a thermal spike model. HRTEM was used to investigate the formation of subgrain boundaries in UO_2 and TEM/SEM as well as the Rutherford backscattering/channeling technique and X-ray diffraction were used to study the polygonized UO_2 and its appearance and structure in detail. Polygonization was also observed in other fuels (advanced and conventional LMFBR fuels (U, Pu)C [8] and (U, Pu) O_2 [9]), in Zr_3Al and U_3Si [10,11], and it has recently also been observed in some minerals [11].

In addition, part of a careful microindentation analysis on different high burnup fuels is reported, which was performed at the ITU hot cells to determine the radial dependence of Vickers hardness, H_v and fracture toughness K_{Ic} . The complete set of microindentation results will be published separately [12]. This study extends results obtained by optical microscopy, TEM and SEM, EPMA and oxygen potential measurements and gives further insight into extent, initiation and formation of the rim structure at increasing burnups.

^{*} Corresponding author. Tel.: +49-7247 951 273; fax: +49-7247 951 590.

The experimental evidence obtained with ion-irradiated UO_2 and with high burnup UO_2 fuels will be used to illustrate the complex set of parameters of importance for grain subdivision of UO_2 . Some technological implications will also be discussed.

2. Experimental

2.1. Ion irradiations

UO_2 single crystals and sinters with 96% of theoretical density and grain sizes of 5–8 μm were polished down to 0.25 μm diamond paste. Subsequently, they were annealed in $\text{Ar}/8\% \text{H}_2$ at 1450°C for 30 min to recover the mechanical damage due to the polishing procedure and to provide high quality surfaces [13]. Rutherford backscattering, RBS, analysis of the single crystals with 2 MeV He-ions, obtained from the van de Graaff accelerator at Forschungszentrum Karlsruhe, Institut für Nukleare Festkörperforschung, in the channeling mode showed minimum aligned yields χ_{\min} near to the theoretically expected values, e.g., $\chi_{\min} = 0.02$ for $\langle 100 \rangle$ oriented crystals at 77 K, thus proving the quality of the crystals.

Ion irradiations were performed at different institutions:

- Forschungszentrum Karlsruhe, Institut für Nukleare Festkörperforschung, Germany (Dr O. Meyer, Dr G. Linker, Dr A. Turos), with Xe-, I- and Cs-beams up to 500 keV energy;
- Atomic Energy of Canada Ltd., Chalk River Laboratories, Canada (Dr R.A. Verrall, Dr P.G. Lucuta and Dr J. Forster), with I-ions of fission energy, 72 MeV;
- Gesellschaft für Schwerionenforschung, GSI Darmstadt, Germany (Dr C. Trautmann and Dr J. Vetter), Xe- and U-ions with very high energies up to 2.7 GeV;
- Hahn Meitner Institut, Berlin, Ionen-Strahl-Labor, ISL (Dr S. Kläumünzer), Xe-ions of 173 MeV.

Following irradiation, the UO_2 samples were analyzed with X-ray diffraction including the techniques of rocking curves and omega-scans [14] to obtain the width of the spread of the small subgrains formed following polygonization, with transmission and scanning electron microscopy and with the above mentioned RBS/channeling techniques. Some of the samples were isochronally annealed at different temperatures to observe damage recovery.

2.2. Microhardness and fracture toughness measurements of high burnup LWR fuel

The fuel samples analyzed in this paper were taken from standard PWR fuel rods which were irradiated in a commercial power reactor for several cycles. The cross-sections chosen correspond to the maximum power positions of different fuel rods. Cladding and fuel materials were zirconium base alloys and UO_2 with initial enrich-

ments between 3.5 and 4.2 w/o U-235. The nominal fuel rod diameter was 10.75 mm, the fuel density was 10.40 Mg/m^3 and the as-fabricated grain size was 7–10 μm . For the present study three fuels with average burnups 40.3, 56.9 and 66.6 GWd/tM were selected.

For sample preparation, ceramographic cross-sections were carefully prepared in several grinding and polishing steps with hard abrasives (SiC and diamond) down to a surface roughness of about 1 μm , with two final polishing steps with submicron oxide suspensions to eliminate as much as possible the surface stresses created during grinding. In addition, two intermediate vacuum reimpregnations were performed between the coarsest grinding steps in order to avoid artificial pore coarsening and grain fragmentation during preparation.

Room temperature microindentation tests at loads of 20, 50 and 100 g were performed with an indentation device of a remote controlled microscope in the hot-cells of the institute, using a Vickers diamond pyramid with an edge angle of 136°. The test conditions consisted of loading and unloading rates of 10 g/s, and a hold-time at load of 5 s. The load was determined on the calibrated scale of an incorporated load cell with a precision of $\pm 2\%$. The diagonals of the resulting indentations and the lengths of the cracks emerging from the indentations were measured on the transferred video image of the imprint, with a precision of about $\pm 0.5 \mu\text{m}$. Determinations of imprint diagonals and crack lengths were done 24 h after the tests, to allow possible strain-relaxation and post-test crack growth processes to be stabilized. Detailed post-test analyses of the imprint areas were performed by optical microscopy and SEM examinations.

For all samples studied, measurements were done on four orthogonal radii, with a separation between indentations of about 8 diagonals at 20 g load, and of about 3 diagonals at 100 g load. The results given are thus the average of four separate measurements, the error bands being placed at the 95% confidence level. The hardness was calculated with the expression [15]

$$H_v = 18.19P/d^2 \text{ GPa,}$$

where P (g) is the indentation load and d (μm) the imprint diagonal. The fracture toughness was calculated via the relationship [16]

$$K_{Ic} = 0.057H_v a^{1/2} (E/H)^{0.4} (c/a)^{-3/2} (\text{MPa m}^{1/2}),$$

where E (MPa) is the Young Modulus, a (m) the half diagonal of the imprint and c (m) the crack length measured from the imprint center.

For crack counting no rejection criterion was applied. Rather, all cracks were evaluated using their largest projection onto any of the two diagonal axes. In case of lateral crack formation and crack branching, like in most of the present indentations on high burnup UO_2 fuel [12], the so-derived (effective) crack lengths tend to underestimate

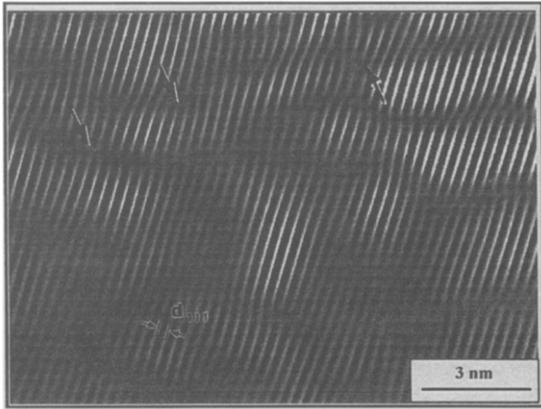


Fig. 1. HRTEM observations on UO_2 irradiated with 500 keV Xe at room temperature. Shown is a Fourier filtered image [20] of the HRTEM micrograph yielding lattice plane images and showing that edge dislocations (see arrows) form subgrains with slightly different orientations (1° – 2°).

the true crack extensions, leading to comparatively higher K_{Ic} values than in the case of straight crack propagation under the same energy dissipation. This is consistent with the intuitive concept that crack path deviation and branching may contribute to an increased material toughness [16].

3. Results

3.1. Ion irradiated UO_2

Previous work (e.g., [17,18]) using ion implantation of UO_2 single crystals with Xe- or I-beams and the RBS/channeling technique had yielded relevant informa-

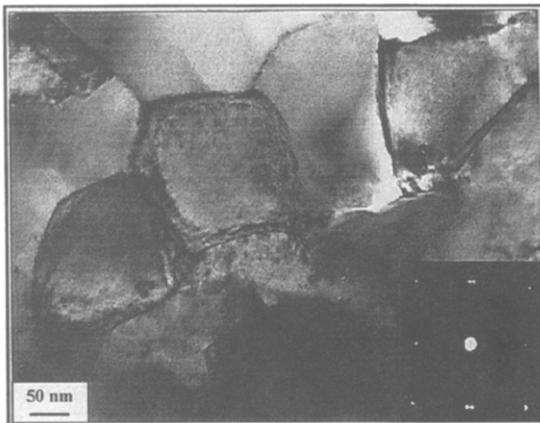


Fig. 2. Transmission electron micrograph showing the structure at the fuel rim of UO_2 with a cross-section average burnup of 74 GWd/tM. The inset diffraction pattern shows the spread in subgrain orientations to be very small.

tion on defect formation in UO_2 . These studies revealed that U-interstitials are mobile below room temperature and that instantaneous defect recovery in UO_2 is very effective: at an ion dose causing about 1 displacement per atom (dpa) in UO_2 , about 95% of the displaced U-atoms jump back into a U-position in the UO_2 lattice. At a damage level of 100 dpa, more than 99.8 of the U-defects recover instantaneously. This high instantaneous recovery rate explains why UO_2 does not get amorphous under the impact of energetic heavy ions, in contrast to many other materials like Al_2O_3 , TiO_2 , SiC etc. (see, for example, [19]). However, polygonization can easily be achieved (e.g., [2,14]) by implanting non-soluble fission products (Xe, I). The results show clearly that a well-defined threshold dose has to be surpassed in order to form the small polycrystals in

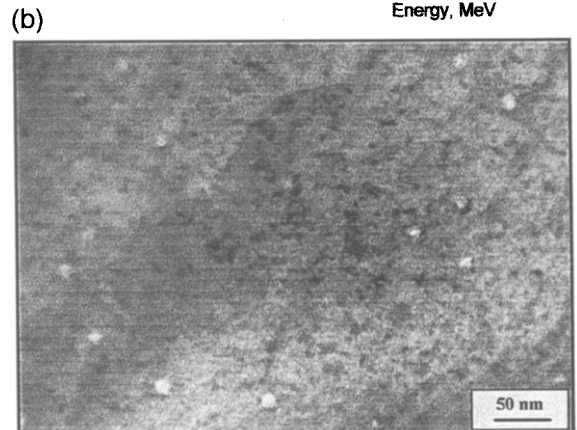
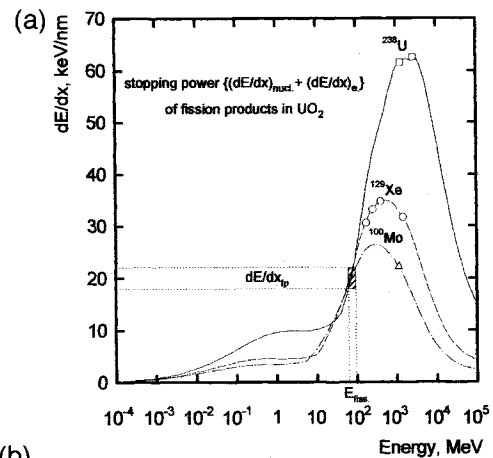


Fig. 3. (a) Calculations with the TRIM code [22] of stopping powers dE/dx of different high energy ions (typical light and heavy fission product ions, Mo and Xe, and U ions) in UO_2 . The energy and the dE/dx ranges for fission products (at the surface of ion-irradiated specimens) are shown as a dashed box. The symbols along the curves show the experimental conditions used so far [23]. (b) TEM micrograph showing a UO_2 sample irradiated with 1300 MeV U-238 ions with a fluence of 5×10^{16} ions/ m^2 [23].

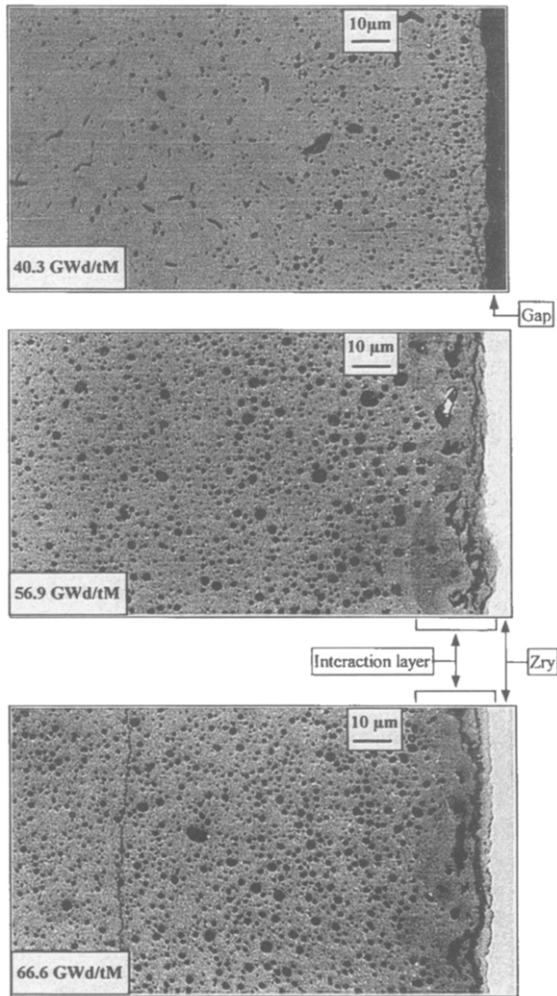


Fig. 4. Optical micrographs of PWR fuels with different burnups. Shown is the pellet periphery. The formation and the inward extension of the rim zone at increasing burnup are clearly seen.

the implanted layer of single crystals of UO_2 . This threshold, i.e., the critical dose for polygonization, corresponds to a fission product concentration reached in a reactor in the burnup range of about 5–7 at.%. X-ray diffraction (ω -scans) showed that the misalignment between the new crystals was small (~ 1 to 2° only). The proposed mechanism for this type of polygonization was fracture and cleavage starting from overpressurized fission product bubbles with pressures of the order of 10^4 bar.

Recent high resolution transmission electron microscopy, HRTEM, of UO_2 irradiated with Xe of higher energy (0.5 MeV) showed that even in the material through which most of the Xe-ions have passed without being stopped, subgrain boundaries can form due to the pile up of a high density of edge dislocations (see Fig. 1 [20]). Similar small subgrains were also observed by Nogita and Une [21] in high burnup UO_2 . These could act as nuclei

for the formation of the well-developed subgrains in the size range of 150 to 300 nm observed in the rim zone of high burnup UO_2 . A typical example [6] for such fully developed subgrains in a high burnup UO_2 fuel is shown in Fig. 2. Note that in Fig. 1, the dislocation pile-up is not due to a high Xe-concentration. It is rather formed in the electronic stopping part of the ions, i.e., these have ionized and heated the lattice while passing through the UO_2 layer observed in TEM.

To get a deeper insight into the consequences of electronic stopping of fission products, ion irradiations of UO_2 were performed at fission energy, but also at higher and

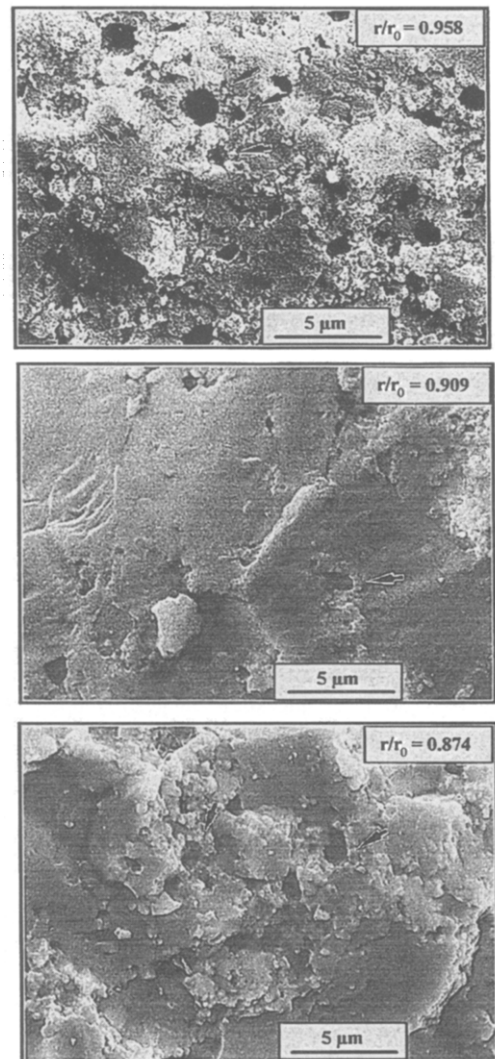


Fig. 5. Microstructural changes in the fuel with 66.6 GWd/tM average burnup as a function of radial location. Part a shows the fully restructured rim, part b the beginning of a transition zone and part c isolated intragranular pores surrounded by small grains (see arrows).

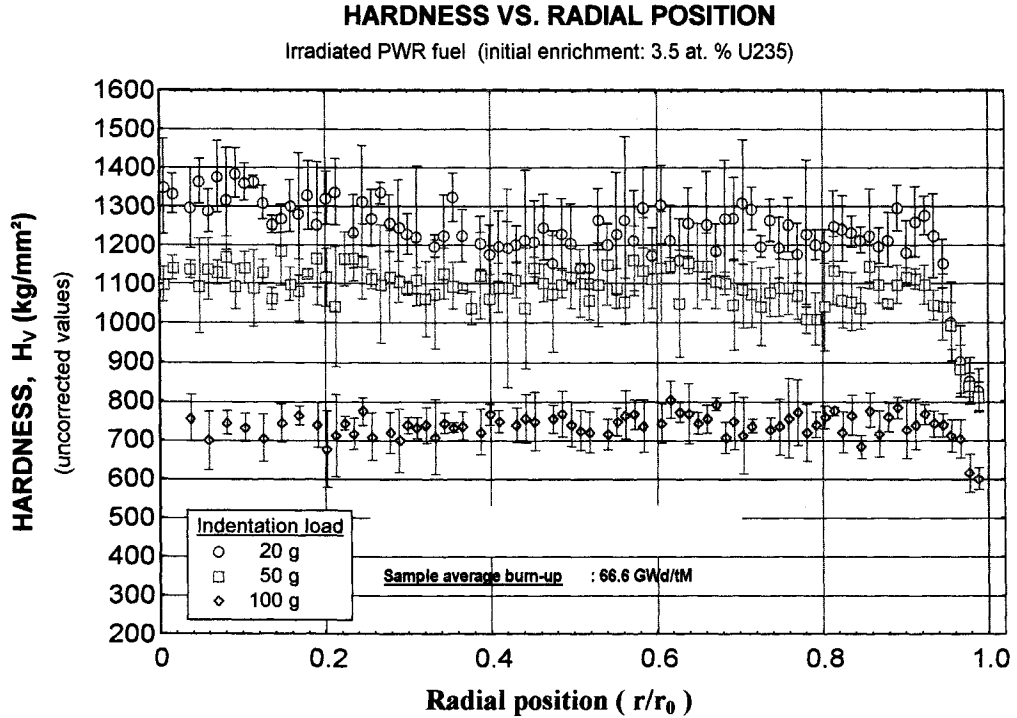


Fig. 6. Radial variation of Vickers hardness H_v for three loads for the fuel of Fig. 5.

lower energies. Fig. 3a shows calculations with the TRIM-95 code [22] of stopping powers of a typical light fission fragment (Mo), a typical heavy fission fragment (Xe) and of U-ions in UO_2 as a function of energy. The conditions for fission are indicated by a dashed box showing the energy range of fission products and their energy loss values in the beginning of their range, and hence at the surface of ion-implanted specimens. TEM analysis of irradiated UO_2 reveals observable tracks for ions with a large stopping power [23]. An example is shown in Fig. 3b (U-238 ions, 1.3 GeV energy, 99.8% electronic stopping, $(dE/dx)_e = 56$ keV/nm, 0.2% nuclear stopping). The measured track radii (~ 5 nm in Fig. 3b), together with known thermodynamic data of UO_2 , can be used to calculate the temperature–time history along the track of the ions, applying a suitable model. The thermal spike model of Toulemonde et al. was used [24] to this end. For the case of Fig. 3b, central temperatures of about 8000 K were obtained. For fission products at fission energy, relatively large volumes heated to above the melting point were calculated. Any given atom of the UO_2 lattice will be affected in this way more than once per day, explaining why damage ingrowth reaches saturation rather fast.

3.2. High burnup PWR fuel: Microhardness and fracture toughness measurements at room temperature

In a previous study [4], the porosity and other relevant features of the microstructure of the rim zone of commer-

cial PWR- UO_2 fuels with average burnups between 40 and 67 GWd/tM had been determined as function of the radial position and the average burnup. This work showed that at the pellet periphery, within a region of few tenths to several hundreds of microns (increasing with burnup), an exponential growth of the fuel porosity and the pore density takes place, resulting in 3 to 4 times larger porosities at the pellet edge, and typically one order of magnitude larger pore densities, compared to the values observed at the onset of the rim zone (Fig. 4). Accompanying the increase in porosity and in pore density, grain subdivision is also evident in the rim zone, leading to a typical

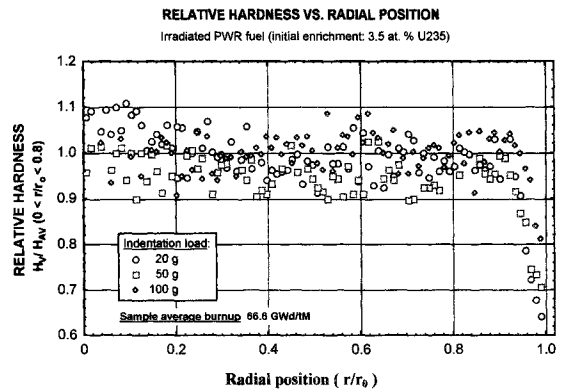


Fig. 7. The data of Fig. 6, normalized to the relatively constant H_v -values observed between $r/r_0 = 0$ and 0.8.

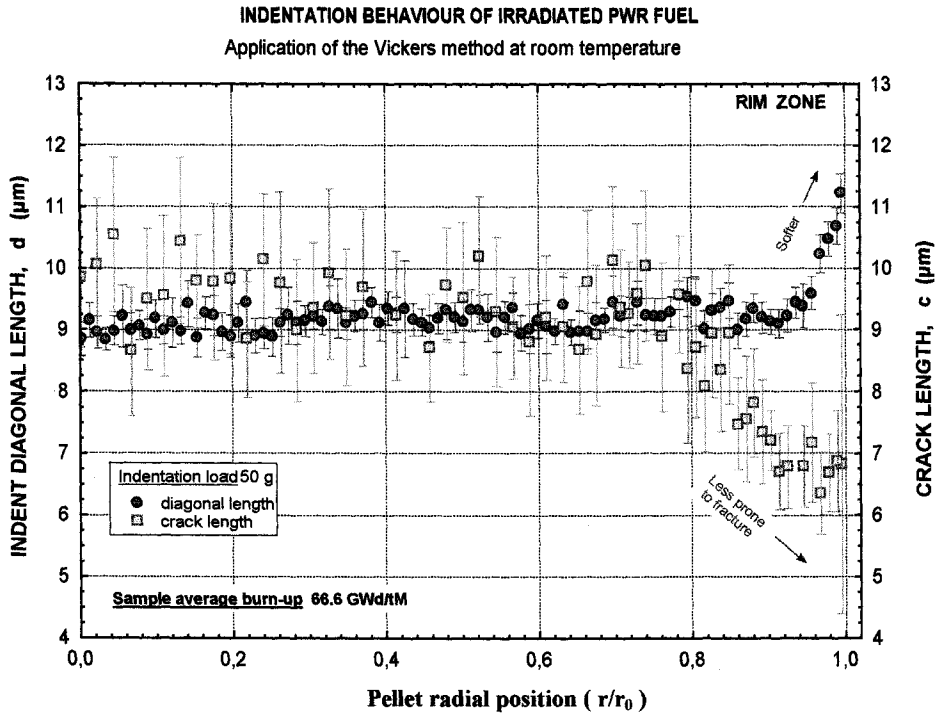


Fig. 8. Radial variation of the diagonal lengths of the indentations, d , and of the crack lengths, c , for the fuel of Fig. 5 (66.6 GWd/tM).

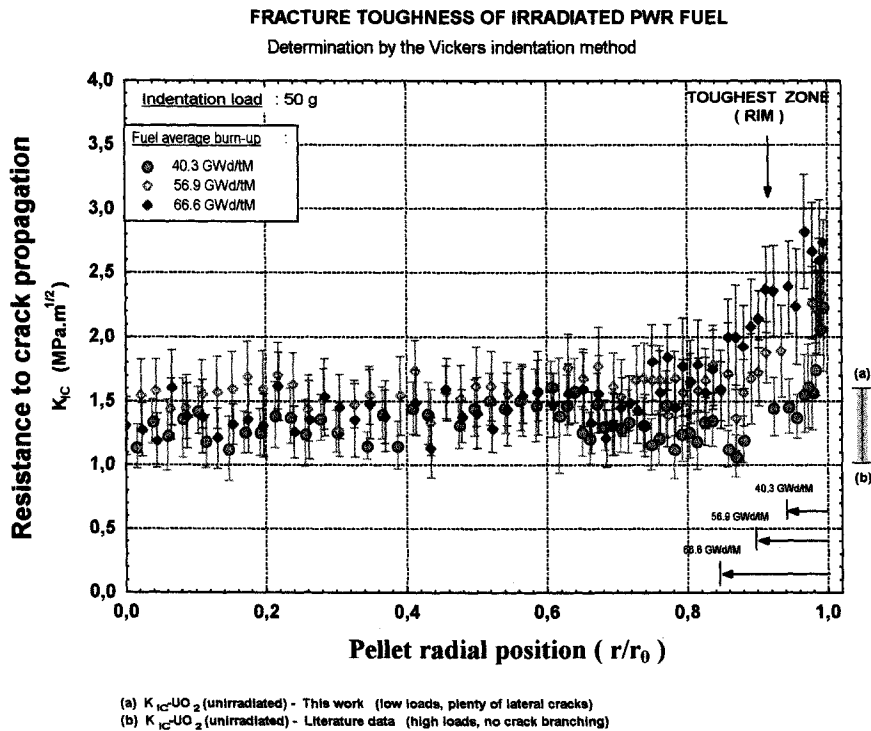


Fig. 9. Radial dependence of the fracture toughness, K_{Ic} of the three PWR fuels of Fig. 4. The bar on the right hand side indicates the differences in determining K_{Ic} with the hot cell equipment (low loads) and previous work (high loads), using unirradiated UO_2 .

'submicron' grain structure after irradiation, in contrast to the relatively large grain size of the as-fabricated material (7–10 μm). The characteristic of this 'in-reactor' grain subdivision is that it appears as a homogeneous structure only in a narrow band near the pellet edge, and that it is observed only locally concentrated around pores further in the fuel [4]. Typical examples of the structure at different radial positions of the fuel with the highest burnup are shown in Fig. 5.

The cross-sections of the three fuels the rim zones of which are shown in Fig. 4 were analyzed with Vickers microindentations to determine the dependence of hardness H_v and fracture toughness K_{Ic} on radial position and on burnup.

Hardness: For all three fuel sections examined in this way, the hardness remained relatively constant along most of the pellet radius, with the exception of a peripheral region showing the rim structure. Here, a reduction of up to 30% of the average occurred towards the pellet edge, independently on the indentation load applied and of the average burnup examined. Fig. 6 shows as typical example the results for the fuel with 66.6 GWd/tM. This fact can be better seen in Fig. 7, where the ratio between the local hardness and the average hardness for the 'plateau' in Fig. 6 (range $r/r_o = 0$ to 0.8) is plotted for the same fuel. The increase of the hardness with decreasing loads as observed in Fig. 6 is a typical feature of the Vickers tests if low loads are used [15]. This dependence can be eliminated using an expression of the type $H \propto (P - W)/d^2$, where P and d have the usual meaning given in Section 2.2 and W represents a critical load below which no indentation is produced [15]. Applying this correction, a load independent hardness value can be assigned to each fuel for the region below $r/r_o = 0.8$ ('plateau' of Fig. 7), showing a linear increase with the average burnup of the fuel [25]. Interesting to note is also the fact that the width of the region within which the decrease of the hardness is observed (Figs. 6 and 7), agrees rather well with that of the region where an enhanced porosity of these fuels is observed, i.e., with the rim region [4], for all fuels examined here.

Crack length and fracture toughness: as with H_v , the radial dependence of the lengths of the indentation cracks, c , and the burnup dependence were determined. Fig. 8 shows the variation of the indentation crack lengths with the radial position for the fuel with 66.6 GWd/tM average burnup, together with the variation of the diagonal lengths of the same indentations. Similarly to the hardness profile (Fig. 6), the crack lengths remain relatively constant along most of the pellet radius ($r/r_o = 0$ to 0.8) until they start to decrease on approaching the outer part of the fuel. This indicates a smaller propensity to crack propagation of the outer fuel regions. This fact, in combination with the observed hardness decrease (Figs. 6 and 7) will result in an improvement of the fracture toughness in the rim region. A second important feature is the fact that the shortening of

the crack lengths starts well before any hardness decrease can be measured, suggesting that the toughening effect associated with the rim zone extends beyond the region defined by the porosity increase or by the hardness reduction. The same observations were made on all three different fuels examined.

Fig. 9 shows the K_{Ic} profiles obtained for the three fuels examined at a constant indentation load (50 g), indicating that the width of the toughened zone and the degree of toughening clearly increase with the average burnup. As mentioned before, the 'toughened' rim extends further into the fuel than the corresponding 'softened' region defined by the hardness profile. Fig. 9 also contains K_{Ic} values for unirradiated UO_2 , according to measurements by other authors at much higher loads (1000 g) [26,27], and the control measurements performed in the present study under the same conditions as for the irradiated fuels. These results show primarily that the fracture toughness of the central parts of the fuel roughly corresponds to the range of values for unirradiated UO_2 , while the fracture toughness of the rim zone can be twice as large.

4. Discussion

The technological importance and possible mechanisms of formation of the rim structure have been discussed before (e.g., Refs. [2,4,7,14,21,28,29]). At the IEQES Conference, two modeling approaches were presented and are contained in these Proceedings [30,31]. We have performed electron microscopy and ion irradiation experiments in order to obtain more information on the possible mechanisms. A direct important property change of the rim structure, as compared to UO_2 , is the reduction in thermal conductivity. Incorporation of fission products, and hence increasing burnup, is known to decrease the thermal conductivity λ very significantly. A physical explanation and a pragmatic modeling approach were recently published [32]. A further important decrease in λ is due to the increased porosity in the rim region. This region constitutes thus an effective heat barrier increasing the fuel temperatures. Another matter of concern is the capability of the rim structure to sufficiently retain fission gases, since the gas pressure inside the cladding must not exceed certain critical levels. The gas release from the fuel depends, among another material parameters, on its mechanical properties, i.e., on its ability to withstand internal overpressures in fission gas bubbles without fracture. Also, the mechanical properties of the rim structure play a significant role during power transients, since they determine to a great extent the level of stress relaxation in case of pellet-cladding mechanical interaction, i.e., the possibility for the cladding to survive or to fail during a given power ramp. Therefore, for a thorough evaluation of the in-reactor performance of high burnup fuels, the determi-

nation of its mechanical properties is important, in particular in the rim zone since this zone is in contact with the clad.

A first approach in this direction is to measure the variation of the hardness and fracture toughness along the fuel radius, since these quantities provide primary information on the deformation and fracture properties of the different radial zones which are formed under irradiation. In this paper, a rather extended set of indentation tests at room temperature is reported for three different PWR fuels with increasing degrees of rim structure formation.

4.1. Ion implantation results

Previous work using fission product ions of comparatively low energy (0.1 to 1.5 MeV) (e.g., [2,14,17,18]) had shown that instantaneous defect recovery in UO_2 is very effective, that UO_2 does not become amorphous — as many other ceramics do, e.g., Al_2O_3 , TiO_2 and U_3O_8 — and that polygonization occurs at well defined threshold fluences of Xe- or I-ions. Polygonization could be produced at 77 K, at room temperature and at 772 K. The suggested mechanism was cleavage and fracture due to overpressurized bubbles of these insoluble fission products. The new work presented here shows that subgrain boundaries in UO_2 can also be formed by largely electronic energy deposition, i.e., with only very small amounts of Xe being stopped in the investigated specimen. Ion implantation was also extended to very high energies (up to 2.6 GeV) and, for the first time, ion tracks could be observed in bulk UO_2 . Again, these were formed at ion energies causing essentially only electronic excitation of UO_2 . With such experiments, the technologically interesting energy range of 70–100 MeV of fission products during fission can be approached from both low and high energies. Of course, ion irradiation can also be performed at the proper fission energy. This is done at JAERI [33] and at our institute, in cooperation with Chalk River, AECL, Canada (Dr R.A. Verrall and Dr P.G. Lucuta).

The material in the rim of high burnups UO_2 is crystalline, near-stoichiometric UO_2 with an oxygen potential of about -400 kJ/mol at 700°C [34,35]. This value proves that no oxidation took place due to fission. However, the fuel in the rim region contains a large amount of soluble fission products and is thus not directly comparable to pure UO_2 . For this reason, simulated high burnup UO_2 , Simfuel, will be used in future work in parallel to experiments on UO_2 . The present results are thus a necessary, but intermediate step towards fully understanding the behavior of high burnup UO_2 . They show that small subgrains can be formed without large amounts of insoluble fission products. Note that full polygonization has not been achieved so far under these conditions (0.5 MeV Xe, thin TEM foil). However, the dose range used so far was limited. The observation of visible ion tracks produced by high energy heavy ions (see Fig. 3b) suggests and confirms

that continuous remelting of material along the fission spikes occurs thus pointing to early saturation in point defect concentration, which is also compatible with the measured large rate of instantaneous defect recovery. This leaves essentially the formation of dislocations, loops, networks and resulting subgrains boundaries, and the lattice strain induced by soluble fission products (e.g., rare earths) as candidates to cause the grain subdivision in UO_2 ion-irradiated to high doses, or in high burnup UO_2 , in addition to the (usually overpressurized) precipitates of insoluble, volatile fission products.

4.2. Microhardness and fracture toughness of high burnup LWR fuel

The present results obtained with fuel stored for a few years after irradiation show that the rim zone in high burnup PWR fuels is associated with a hardness decrease of about 30% and with a fracture toughness increase of about 100% with respect to the rest of the fuel. While the variation of hardness correlates well with the local increase of porosity within the rim zone, the variation of toughness apparently extends further beyond the porous region at the rim. That hardness decreases almost monotonically with the degree of porosity is a normal feature in ceramic materials [36], which was also reported for unirradiated UO_2 and (U, Pu) O_2 [37]. This may indicate that the predominant effect on the hardness of the rim material is due to the increased porosity, since the other two important characteristics of this zone, i.e., the increased local burnup and the refined grain size, would act just in the opposite way. The increase in H with burnup is evidenced by the present results on the fuel regions outside of the rim region and by previous results on simulated burnup UO_2 , so-called Simfuel [38]. The increase with decreased grain size would be expected due to a type of Hall–Petch strengthening mechanism [36,39,40].

The increase in K_{Ic} at the rim is unexpected since most of the experimental evidence on other ceramics points to a decrease in K_{Ic} with increasing porosity [36,40–42], the opposite dependence to the one observed here. However, the increase in K_{Ic} could probably be attributed to the smaller grain size in the rim zone. Ceramics with submicron grain size can be expected to have an increased ductility at the crack tip (plastic zone [43]). If this were the case, the observed improvement in K_{Ic} beyond the porous region of the rim zone would suggest that some grain refinement occurs before any pore formation and bulk grain subdivision becomes noticeable.

Finally, an overall idea of the improvement of the mechanical properties of the rim zone can be obtained by evaluating the ‘brittleness parameter (H/K_{Ic})’, as suggested by Lawn and Marshall [44,45]. If this is done, the unirradiated UO_2 is comparable to hot-pressed SiC . The degree of brittleness is improved in the rim zone by 50% compared to unirradiated UO_2 , bringing high burnup UO_2 towards the tougher ceramics such as hot-pressed Si_3N_4 .

The above discussion has not considered a potentially important point. Measurements on high burnup fuel are made a few years after the end of irradiation, following a storage period at relatively low temperatures. Due to the high burnup, in particular in the (neutronic) rim zone, a high concentration of α -emitting, shortlived actinides are formed (Pu-238, Am-241, Cm-242, Cm-244 etc.). It has been shown for many ceramic materials (e.g., waste ceramics like zirconolite $\text{CaZrTi}_2\text{O}_7$, $\text{Gd}_2\text{Ti}_2\text{O}_7$, $\text{Ca}_2\text{Nd}_8(\text{SiO}_4)_6\text{O}_2$, Synroc etc.) subjected to α -decay damage (e.g., Ref. [46]), and also for ThO_2 irradiated with α -particles [47] that this type of damage shows exactly the same effects as observed here, i.e., a decrease in H by $\sim 30\%$ and an increase in K_{Ic} by up to 100%. Similar effects can be expected for UO_2 . However, since no exact data on α -decay damage in higher actinide containing UO_2 are available at present, a correction of the presented results for α -decay damage could not be made. The present results are thus representative for stored fuel, but not necessarily for fuel under reactor operating conditions.

5. Conclusions

The purpose of this paper is to present new information and experimental results of relevance to the mechanism of formation of the rim structure, i.e., the polygonization or grain subdivision occurring at about 70 MWd/kgM local burnup in UO_2 fuel irradiated below a threshold temperature of about 1000 to 1100°C. The results are helpful for a better understanding of grain subdivision and provide insights towards a modeling of this complex phenomenon. This type of work has to be continued, more careful analyses of the rim of high burnup UO_2 have to be performed and modeling attempts as those presenting during the IEQES meeting and contained in the present proceedings [30,31] have to be continued and extended before a full understanding of the mechanism and of the contributing phenomena and factors can be achieved. The present study is a step forward in this direction.

The presented results show that nucleation of subgrains can be achieved in the absence of large amounts of fission products and by predominantly electronic energy loss. They show also, that mechanical property changes (H , K_{Ic}) do not fully correlate with porosity formation in the rim zone: the changes in fracture toughness extend deeper into the fuel than those of the hardness and than the formation of the typical pores of $\sim 1 \mu\text{m}$ diameter pointing to a nucleation mechanism causing property changes before the coarse pores are formed. This new information, together with the pre-existing knowledge, confirms that grain subdivision is a very complex phenomenon affected by many parameters. On the other hand, it is not restricted to high burnup UO_2 . It has recently been found in high burnup (U, Pu) O_2 [9] and, more importantly, in high burnup (U, Pu)C [8] as well. It is thus not a particular

feature of the fluorite structure. Since more information is becoming and will become available, a final understanding may be achieved in a not distant future.

Acknowledgements

The authors would like to thank a number of colleagues for their contribution, their help and for discussions, mainly M. Coquerelle and his team of the hot cells of ITU for specimen preparation and L.M. Wang (University New Mexico, Albuquerque, USA), I.L.F. Ray and T. Wiss for their high quality electron microscopy. In addition, the authors would like to thank all the scientists mentioned in Section 2.1 for the many ion irradiations performed for this study.

References

- [1] Hj. Matzke, H. Blank, M. Coquerelle, K. Lassmann, I.L.F. Ray, C. Ronchi, C.T. Walker, *J. Nucl. Mater.* 166 (1989) 165.
- [2] Hj. Matzke, *J. Nucl. Mater.* 189 (1992) 141.
- [3] H. Stehle, *J. Nucl. Mater.* 153 (1988) 3.
- [4] J. Spino, K. Vennix, M. Coquerelle, *J. Nucl. Mater.* 231 (1996) 179.
- [5] M.E. Cunningham, M.D. Freshley, D.D. Lanning, *J. Nucl. Mater.* 188 (1992) 19.
- [6] I.L.F. Ray, Hj. Matzke, H.A. Thiele, M. Kinoshita, *J. Nucl. Mater.* 245 (1997) 115.
- [7] K. Une, K. Nogita, S. Kashibe, M. Imamura, *J. Nucl. Mater.* 188 (1992) 65.
- [8] I.L.F. Ray, Hj. Matzke, *J. Nucl. Mater.*, in press.
- [9] K. Maeda, T. Mitsugi, T. Asaga, presented at Int. Workshop on Interfacial Effects in Quantum Engineering Systems (IEQES-96), Mito, Japan, Aug. 21–23 1996.
- [10] R.C. Birtcher, L.M. Wang, *Nucl. Instrum. Methods B59&60* (1991) 966.
- [11] L.M. Wang, R.C. Birtcher, R.C. Ewing, *Nucl. Instrum. Methods B80&81* (1993) 1109.
- [12] J. Spino et al., *J. Nucl. Mater.* 231 (1998) 179.
- [13] Hj. Matzke, A. Turos, *J. Nucl. Mater.* 114 (1983) 349.
- [14] Hj. Matzke, A. Turos, G. Linker, *Nucl. Instrum. Methods B91* (1994) 294.
- [15] A. Jain, A.K. Razdan, P.N. Kotru, B.M. Wanklyn, *J. Mater. Sci.* 29 (1994) 3847.
- [16] Hj. Matzke, *Indentation Fracture and Mechanical Properties of Ceramic Fuels and of Waste Ceramics and Glasses* (Harwood Academic, Chur) special issue of *Eur. Appl. Res. Reports: Nucl. Sci. Techn.* 7 (1987).
- [17] Hj. Matzke, A. Turos, *J. Nucl. Mater.* 188 (1992) 285.
- [18] Hj. Matzke, *Nucl. Instrum. Methods B65* (1992) 30.
- [19] Hj. Matzke, *Radiat. Eff.* 64 (1982) 3.
- [20] Hj. Matzke, L.M. Wang, *J. Nucl. Mater.* 231 (1996) 155.
- [21] N. Nogita, N. Une, *J. Nucl. Mater.* 226 (1995) 302.
- [22] J.F. Ziegler, J.P. Biersack, U. Littmark, *The Stopping and Range in Solids* (Pergamon, Oxford, 1985).
- [23] T. Wiss, Hj. Matzke, C. Trautmann, M. Toulemonde, S.

- Klaumünzer, Proc. E-MRS meeting Strasbourg, June 1996, Nucl. Instrum. Methods B122 (1997) 583.
- [24] M. Toulemonde, E. Paumier, C. Dufour, *Radiat. Eff. Def. Solids* 126 (1993) 205.
- [25] J. Spino, Hj. Matzke, to be published.
- [26] T.G.R. Kutty, A.K. Sengupta, C. Ganguly, in: *Indentation Techniques*, eds. Hj. Matzke and E. Toscano (Harwood Academic, Chur, 1990) p. 1473.
- [27] Hj. Matzke, R. Forst, to be published.
- [28] K. Nogita, K. Une, *Nucl. Instrum. Methods B91* (1994) 301.
- [29] K. Nogita, K. Une, M. Hirai, K. Ito, K. Ito, Y. Shirai, these Proceedings, p. 196.
- [30] M. Kinoshita, these Proceedings, p. 185.
- [31] J. Rest, these Proceedings, p. 180.
- [32] P.G. Lucuta, Hj. Matzke, I.J. Hastings, *J. Nucl. Mater.* 232 (1996) 166.
- [33] K. Hayashi, H. Kikuchi, K. Fukuda, these Proceedings, p. 191.
- [34] Hj. Matzke, *J. Nucl. Mater.* 208 (1994) 18.
- [35] Hj. Matzke, *J. Nucl. Mater.* 223 (1995) 1.
- [36] R.W. Rice, in: *Treatise of Materials Science and Technology*, Vol. 11, ed. R.K. MacCone (Academic Press, New York, 1977) pp. 200.
- [37] G. Engelhard, H. Hofmann, German report KFK 729, 1968.
- [38] Hj. Matzke, P.G. Lucuta, R.A. Verrall, R. Forst, R. Mele, to be published.
- [39] A. Krell, P. Blanck, *J. Am. Ceram. Soc.* 78 (1995) 1118.
- [40] R.W. Rice, C.C. Wu, F. Borchelt, *J. Am. Ceram. Soc.* 77 (1994) 2539.
- [41] R.W. Rice, S.W. Freiman, in: *Ceramic Microstructures*, ed. R. Fulrath, Vol. 76, 6th Int. Material Conf., Berkeley, CA, 1976, p. 800.
- [42] R.W. Rice, *Mater. Sci. Eng. A112* (1989) 215.
- [43] M. Mayo, *Mechanical Properties and Deformation Behaviour of Materials Having Ultrafine Microstructures*, eds. M. Natasi et al. (Kluwer Academic, Dordrecht, 1993) p. 361.
- [44] B.R. Lawn, D.B. Marshall, *J. Am. Ceram. Soc.* 62 (1979) 347.
- [45] D.B. Marshall, B.R. Lawn, in: *Indentation of Brittle Materials*, ASTM STP 889, eds. P.J. Blau and B.R. Lawn (ASTM, Philadelphia, PA, 1986) p. 26.
- [46] W.J. Weber, Hj. Matzke, in: *Indentation Fracture and Mechanical Properties of Ceramic Fuels and of Waste Ceramics and Glasses*, ed. Hj. Matzke, Vol. 7, Special issue *Europ. Appl. Res. Rep.* (1987) p. 1221.
- [47] Hj. Matzke, J.L. Routbort, *J. Nucl. Mater.* 115 (1983) 334.